



**HAL**  
open science

# Nuclear-magnetic-resonance diffusion simulations in two phases in porous media

A. Valfouskaya, P. M. Adler

► **To cite this version:**

A. Valfouskaya, P. M. Adler. Nuclear-magnetic-resonance diffusion simulations in two phases in porous media. *Physical Review E*, 2005, 72, pp. 253-269. 10.1103/PhysRevE.72.056317. insu-03601104

**HAL Id: insu-03601104**

**<https://insu.hal.science/insu-03601104>**

Submitted on 8 Mar 2022

**HAL** is a multi-disciplinary open access archive for the deposit and dissemination of scientific research documents, whether they are published or not. The documents may come from teaching and research institutions in France or abroad, or from public or private research centers.

L'archive ouverte pluridisciplinaire **HAL**, est destinée au dépôt et à la diffusion de documents scientifiques de niveau recherche, publiés ou non, émanant des établissements d'enseignement et de recherche français ou étrangers, des laboratoires publics ou privés.

**Nuclear-magnetic-resonance diffusion simulations in two phases in porous media**

A. Valfouskaya and P. M. Adler\*

*Institut de Physique du Globe de Paris (IPGP), Laboratoire des Milieux Poreux et Fracturés, Boîte 89, 4 place Jussieu, 75252 Paris Cedex 05, France*

(Received 24 June 2005; published 15 November 2005)

Time-dependent diffusion simulations which can be measured by nuclear magnetic resonance (NMR) were numerically performed in consolidated reconstructed porous media saturated by two immobile fluids. The phase distributions were obtained by an immiscible lattice Boltzmann technique which incorporates interfacial tension and wetting. The apparent diffusion coefficient in each fluid was determined by a random walk algorithm. Permeability and conductivity tensors were calculated by finite-difference schemes. The major properties valid for a single phase could be generalized to two phases. First, the characteristic length  $\Lambda$  introduced by Johnson *et al.* [Phys. Rev. Lett. **57**, 2564 (1986)] is of the order of twice the phase volume to surface ratio. Second, the apparent diffusion coefficients for all porosities, saturations, and phases can be represented by a single dimensionless curve.

DOI: [10.1103/PhysRevE.72.056317](https://doi.org/10.1103/PhysRevE.72.056317)

PACS number(s): 47.55.Mh, 47.55.Kf, 81.05.Rm, 47.11.+j

**I. INTRODUCTION**

Multiphase flows through porous media have received a lot of attention because of their fundamental and industrial importance. Experimental study of such phenomena is made easier by NMR because it is a nonintrusive technique and because it can provide information on crucial quantities such as saturation. A recent example of the application of NMR is due to [2].

The main objective of this paper is to perform numerical simulations of NMR in porous media saturated by two immobile fluids. Though relaxation effects will be neglected in this study, it is useful to describe them briefly. Under the usual circumstances, relaxation due to the solid interface is much larger than the one due to the fluid-fluid interface [3]. Therefore, the wetting fluid relaxes first and then the nonwetting one. During experiments, the signals coming from the two fluids can be distinguished, but this often demands costly efforts [4]. Numerical simulations have an advantage in this situation, since these signals can be calculated for each fluid independently.

Only Toumelin *et al.* [5] performed numerical simulations of nuclear magnetic resonance in model porous media saturated by two fluids. In addition to surface relaxation, the authors took into account bulk relaxation and relaxation due to internal magnetic field gradients. Such internal magnetic field gradients originate from the interactions between the external static magnetic field and the solid grains of the porous media due to irregularities in the pore space, together with a contrast between the solid and fluid susceptibilities [3]. The porous medium was schematized by a simple cubic array of spheres (see also [6]). The pores were filled with water. Blobs of oil were added at the corners of the cell, and the configuration was spatially periodic. To obtain micropores inside the spherical grains, the grain was divided into smaller cells in which, inversely, the pore was a sphere

at the center and all the rest of the small cell was filled with water. Surface relaxation could occur at solid-fluid interfaces. The fluid-fluid interfaces had zero relaxation strength.

The present study is restricted to a diffusion process without any relaxation. The particles representing the fluid molecules are specularly reflected from the fluid-fluid interfaces in the same way as from the fluid-solid ones. The diffusion process is simulated in each fluid separately by the random walk algorithm already used by [6]. The emphasis is put on the apparent diffusion coefficient. Moreover, the porous media used here reproduce the statistical properties (porosity and correlation function) of some real porous media such as sandstones.

The diffusion process is simulated in each fluid phase, filling the media when the fluids are immobile. The two phase configurations are determined for various porosities and saturations. The configurations are calculated by an immiscible lattice Boltzmann algorithm [7,8] with periodic boundary conditions; i.e., the fluid which leaves one side of a sample comes back by the opposite one.

Simulations are performed on samples of unimodal porous media which are homogeneous and isotropic with a single correlation length (Sec. II A). Though the pore space is isotropic, the phase configuration is not necessarily isotropic because of the pressure gradient which was initially applied and of their subsequent return to interfacial equilibrium.

The apparent diffusion coefficient of each fluid phase is studied in the same manner as in [6]. For two fluids, it may also serve as an indicator of the continuity of the phases. If it tends to zero in some direction, it means that the mean-square displacement of the fluid molecules is bounded by a solid surface or an interface with another fluid and that the fluid does not percolate along this direction.

**II. GENERAL**

Consider a porous medium saturated with two fluids—namely, oil and water. Let us assume that water is the wetting phase.

\*Corresponding author. Electronic address: [adler@ipgp.jussieu.fr](mailto:adler@ipgp.jussieu.fr)

The apparent diffusion coefficient is determined when the fluids are motionless. In this equilibrium configuration, the wetting fluid is mostly located close to the surface of the solid.

The walkers represent the fluid molecules. Diffusion is modeled by their random displacements within a given fluid domain limited by the solid matrix and some different fluid phase or interface. When the walkers fall onto such solid or fluid interfaces, they undergo specular reflection without any relaxation.

### A. Porous media

The samples used for this work are the samples of the homogeneous and isotropic unimodal porous media, reconstructed according to the algorithm proposed by Adler *et al.* [9]. Let us describe briefly the reconstruction process. A real porous medium can be described by a phase function

$$Z(\mathbf{x}) = \begin{cases} 1, & \text{if } \mathbf{x} \text{ belongs to the pore space,} \\ 0, & \text{otherwise.} \end{cases} \quad (1)$$

The two major average properties of the medium are

$$\varepsilon = \overline{Z(\mathbf{x})}, \quad (2a)$$

$$R_Z(\mathbf{u}) = \frac{\overline{[Z(\mathbf{x}) - \varepsilon][Z(\mathbf{x} + \mathbf{u}) - \varepsilon]}}{\varepsilon - \varepsilon^2}, \quad (2b)$$

where  $\varepsilon$  is the porosity,  $\mathbf{u}$  a translation vector, and  $R_Z(\mathbf{u})$  the correlation function of  $Z(\mathbf{x})$ .

The porosity  $\varepsilon$  and the correlation function  $R_Z(\mathbf{u})$  can be measured on thin sections of real media. Then, a random field  $Z(\mathbf{x})$  can be generated such that Eqs. (2) hold. It can be shown [9] that it can be derived from a random Gaussian field  $X(\mathbf{x})$  successively passed through a linear filter [which results in a correlated Gaussian field  $Y(\mathbf{x})$ ] and a nonlinear one [which results in  $Z(\mathbf{x})$ ]. The correlation function of  $Y(\mathbf{x})$  is imposed. For the media considered here, it is equal to

$$R_Y(\mathbf{u}) = \exp\left(-\left(\frac{\pi u}{l_p}\right)^2\right), \quad (3)$$

where  $l_p$  is the correlation length of the pores and  $u = \|\mathbf{u}\|$ .

When a real medium is statistically homogeneous, it can be represented by a cell of finite size, translated periodically along three orthogonal axes. This unit cell in its turn can be discretized into elementary cubes of side  $a$ , such that each cube is either entirely filled with solid or is empty; i.e., it represents the pore space. Along each side of this cell, there are  $N_c$  elementary cubes. Thus, the cell contains  $N_c^3$  elementary cubes and its volume is  $(N_c a)^3$ .

Samples of porosity  $\varepsilon = 0.2, 0.3$  and  $0.4$  discretized by  $N_c = 32$  elementary cubes will be used. The correlation length  $l_p$  is equal to 15. The samples are represented in Figs. 1(a)–1(c).

It should be noted that porous media can be reconstructed in various ways. For instance, grain reconstruction was proposed by [10] which is well suited for low-porosity sandstones. Long-range correlations were introduced by [11].

### B. Equilibrium phase configurations and notations

The diffusion-relaxation process should be simulated over an equilibrium configuration when the two fluids are motionless. To obtain such an equilibrium configuration, fluids are first moved under a pressure gradient. Then, this pressure gradient is suppressed and the fluids continue to move for some time under the action of capillary forces before they stop.

The motion of two fluids is simulated by an immiscible lattice Boltzmann (ILB) algorithm [7,8]. Interfacial tension and wetting are incorporated in this code. Here, water is supposed to be the wetting fluid.

Let us describe how the equilibrium configurations are obtained in three steps by the ILB algorithm. First, the two fluids are arbitrarily placed in two parallel slices [see Fig. 2(a)]. Then, a constant-pressure gradient  $\overline{\nabla P}$  is applied to the sample and the two fluids begin to move.  $\overline{\nabla P}$  is applied for a time sufficiently long so that the relative permeabilities  $K_{r\alpha}$  ( $\alpha = w, o$ ) reach a stationary state (see Fig. 3). The dimensionless time  $IT_0$ , when this occurs, varies with  $\varepsilon$  and  $S_w$ ; it is equal either to  $4 \times 10^6$  or  $8 \times 10^6$  iterations. Third, after  $IT_0$  iterations,  $\overline{\nabla P}$  is canceled and the two fluids flow under the action of the capillary forces only until they reach equilibrium. Figure 2 shows that during this last step, the phase configuration undergoes significant variations at least at the beginning. Progressively, the variations diminish and an equilibrium configuration is reached. In such a configuration, the total curvature of the interface is constant. Of course, in complex porous structures, such equilibrium configurations are not unique and they depend on the precise way they are obtained.

During the ILB calculations, each fluid is represented by a finite set of  $N_\alpha$  ( $\alpha = w, o$ ) colored particles for water and oil. Therefore, four cases can happen in each elementary cube.

(i)  $N_o = 0$ ; all the volume of the elementary cube is filled with water; the total volume of these cubes is noted by  $V^w$ .

(ii)  $N_w > N_o$ ; the concentration of water is larger than the concentration of oil; the total volume of such cubes is noted by  $V^{wi}$ .

(iii)  $N_w < N_o$ ; the concentration of water is smaller than the concentration of oil; the total volume of such cubes is noted by  $V^{oi}$ .

(iv)  $N_w = 0$ ; all the volume of the elementary cube is filled with oil; the total volume of these cubes is noted by  $V^o$ .

In cases (i) and (ii), the phases in the cubes are pure. In cases (ii) and (iii), the corresponding elementary cubes can be considered as being in the oil-water interface; therefore, the superscript  $i$  standing for interface was included.

Often the majority rule is applied which means that the fluid elementary cubes are of two sorts. In the first one,  $N_w$  is larger than  $N_o$  [(i)+(ii)] and the cube is considered to be filled by water. In the second one,  $N_w < N_o$  [(iii)+(iv)] and the cube is filled by oil. The volumes corresponding to the majority rules are denoted by the superscript  $t$  (for total):

$$V^{wt} = V^w + V^{wi}, \quad V^{ot} = V^o + V^{oi}. \quad (4)$$

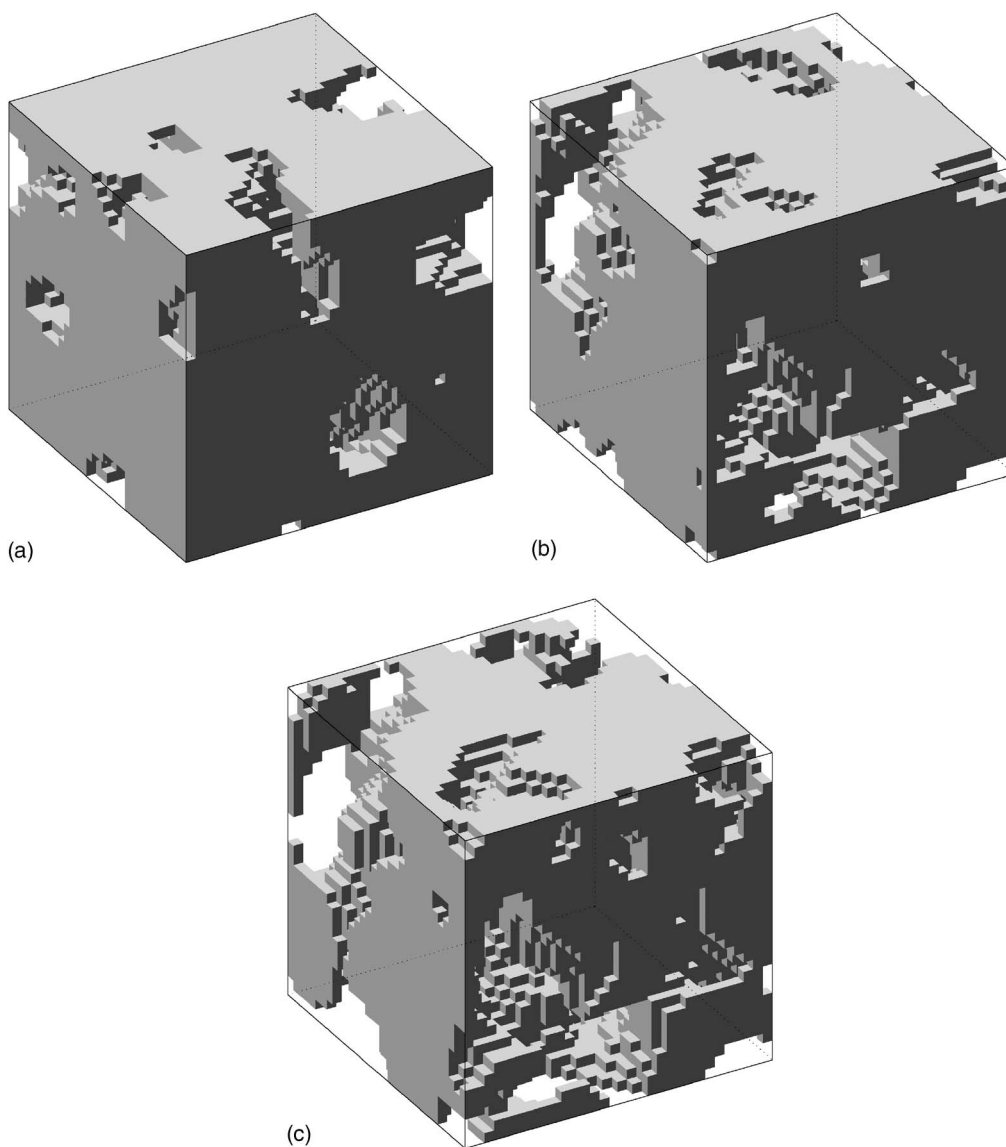


FIG. 1. Samples of porous media discretized by  $N_c=32$  cubes of side  $a$ . Porosity of the samples: (a)  $\epsilon=20\%$ , (b)  $\epsilon=30\%$ , and (c)  $\epsilon=40\%$ .

These four possibilities will be denoted by the index  $\alpha$  which is equal to

$$\alpha = w, wt, ot, o. \tag{5}$$

As a direct application, the saturation of phase  $\alpha$  is defined as

$$S_\alpha = \frac{V^\alpha}{V^p}, \tag{6}$$

where  $V^p$  is the total pore volume.

The interfacial area  $A_\alpha$  of phase  $\alpha$  is equal to the total fluid and solid area bounding phase  $\alpha$ .

This might be the right place to comment on this procedure. As said, the initial configuration perpendicular to  $\nabla P$  is arbitrary and it could be replaced by any other choice. However, it presents the decisive advantage of being simple

and easily reproducible. Configurations simulating imbibition or drainage are much more difficult to obtain. In unpublished studies, various initial configurations were tried with relatively little influence on the results for intermediate saturations.

Finally, it is clearly not the purpose of this work to present relative permeability curves as functions of porosity and saturations. Such curves can be found in [12]. Calculations of the resistivity index were made by [13].

### C. Macroscopic properties of the porous media

Some macroscopic properties of the samples were determined in a systematic way. Geometric properties such as the interfacial areas and the surface-to-volume ratios were calculated for each equilibrium configuration. Moreover, percolation of phase  $\alpha$  along the  $x$ ,  $y$ , and  $z$  directions is characterized by  $p^\alpha(x,y,z)$ . This function is equal to 1 along a

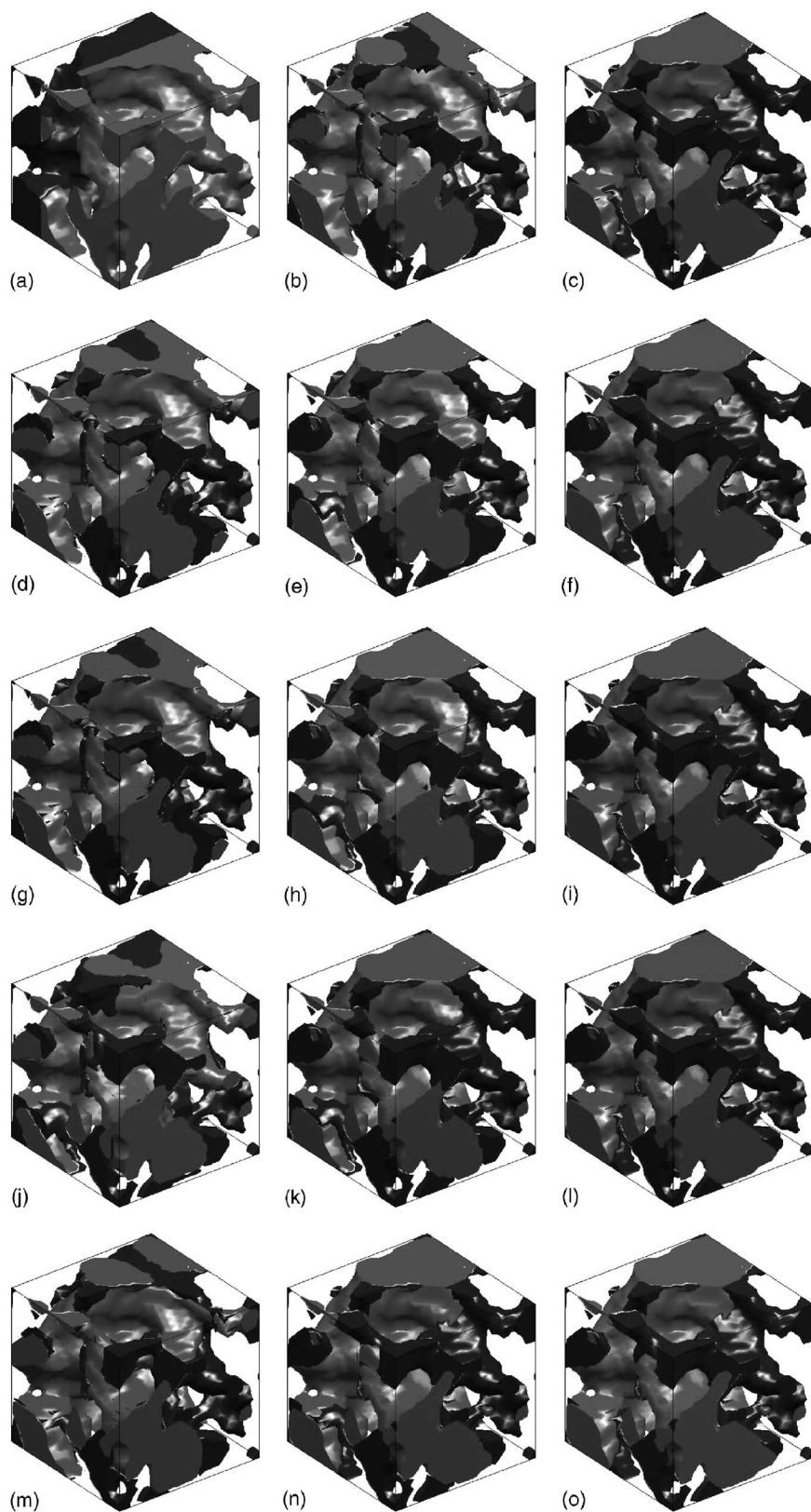


FIG. 2. Determination of an equilibrium configuration for the sample  $\varepsilon=0.4$  with  $S_w=0.4$ . The solid phase is transparent so that only the pore space is seen; water is gray and oil black. (a) corresponds to the initial arbitrary configuration. From (b) to (e), the fluids move under a constant macroscopical pressure gradient  $\nabla P$  parallel to the  $x$  axis. From (f) to (o), the fluids move under the influence of the interfacial tension only. They stop after a large number of iterations (o).

direction if the considered fluid phase is percolating along this direction and 0 otherwise.

The permeability  $K^\alpha$  is determined by solving the Stokes equations in phase  $\alpha$  by a fourth-order finite-difference scheme [14]. Note that during these calculations, a no-slip

boundary condition is also applied to the fluid-fluid interfaces.

The macroscopic conductivity tensor  $\bar{D}^\alpha$  was obtained by solving the Laplace equation in phase  $\alpha$  by a second-order finite-difference scheme [15]. As a by-product,

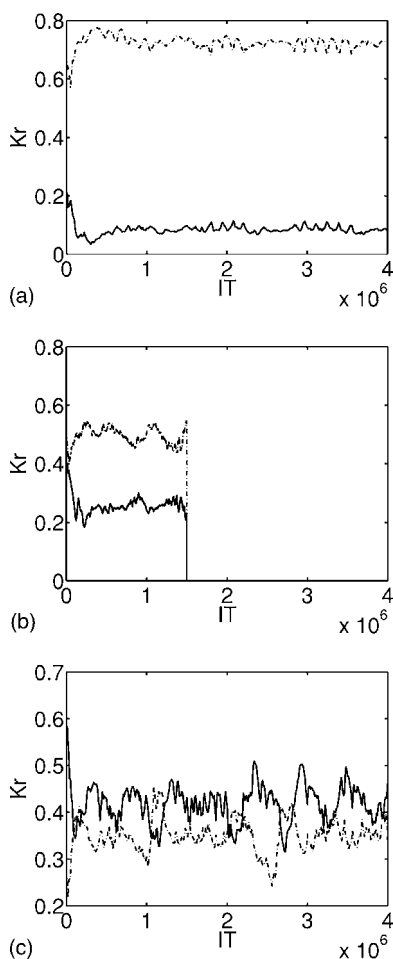


FIG. 3. The relative permeabilities of water (solid line) and oil (dashed line) for the sample of porosity  $\varepsilon=0.4$ . Data are for (a)  $S_w=0.3$ , (b)  $S_w=0.5$ , and (c)  $S_w=0.7$ .

the length scale introduced by [1] is systematically determined:

$$\Lambda^\alpha = 2 \frac{\int_{V^\alpha} |\mathbf{E}^\alpha(\mathbf{r})|^2 dV}{\int_{A^\alpha} |\mathbf{E}^\alpha(\mathbf{r})|^2 ds}. \quad (7)$$

It is essentially a volume-to-surface ratio with a measure weighted by the local value of the electric field  $\mathbf{E}^\alpha(\mathbf{r})$ .  $\Lambda^\alpha$  is determined by the same numerical program as  $\bar{\mathbf{D}}^\alpha$ .

$\bar{\mathbf{D}}^\alpha$  is also equal to the macroscopic diffusion tensor since diffusion is a solution of the Laplace equation as well.  $\bar{\mathbf{D}}^\alpha$  is more often referred to as the conductivity tensor since it is much more convenient to measure conductivity than diffusion.

An alternative characteristic length of a porous medium can be introduced along the  $i$  axis,  $i=x,y,z$ :

$$\Lambda_i^\alpha = \sqrt{8K_{ii}^\alpha F_{ii}^\alpha}, \quad (8)$$

where  $F_{ii}^\alpha = (\bar{D}_{ii}^\alpha / D_m^\alpha)^{-1}$  is the formation factor along the axis  $i$ . For an isotropic porous medium, this length ( $\Lambda = \sqrt{8KF}$ )

was proposed by [16,17] as a way to determine  $K$ .

#### D. Random walk algorithm

As already stated, only diffusion is taken into account and the diffusing particles are supposed to be located in a single phase. Four choices can be made depending on the definition of the initial volume which can be  $V^w$ ,  $V^{wt}$ ,  $V^{ot}$ , or  $V^o$ .

Let us detail this algorithm. A large number of particles,  $N_p$ , is released in the chosen phase at time zero. The initial distribution is uniform. During all the subsequent elementary time steps  $\delta_t$ , the position of each particle  $i$  is updated by a displacement  $\delta_D$  of a given modulus  $\delta_D = |\delta_D|$ , but of a random direction

$$\mathbf{x}_i(t + \delta t) = \mathbf{x}_i(t) + \delta_D, \quad (9)$$

where  $\mathbf{x}_i(t)$  is the position at time  $t$  and  $\mathbf{x}_i(t + \delta t)$  the position at time  $t + \delta t$ .

The modulus  $\delta_D$  of the random jump is constant and related to the molecular diffusivity  $D_m$  by

$$\delta_D^2 = 6D_m \delta t. \quad (10)$$

In all calculations,  $\delta_D$  should be small when compared to the size  $a$  of the elementary cube. However, as shown by [6], the following value gives satisfactory results:

$$\delta_D = 0.4a. \quad (11)$$

If the particle falls onto a boundary, its clock is incremented by a fraction of  $\delta t$ :

$$\mathbf{x}_i(t + \lambda \delta t) = \mathbf{x}_i(t) + \lambda \delta_D, \quad 0 \leq \lambda \leq 1, \quad (12)$$

which corresponds to the intersection of the path and boundary. At the subsequent time step, the particle starts from this location. Since particles close to the walls may accumulate time delays at regular time intervals, these delayed particles are allowed at periodic intervals to catch up with time. Note that the boundary contains the solid phase and the elementary liquid cubes which do not belong to the initial volume as defined at the beginning of this subsection.

Since the fluid phase through which the random walk simulations are performed can be anisotropic, the apparent diffusion coefficient in phase  $\alpha$  is defined as a  $3 \times 3$  tensor [18]

$$\mathbf{D}^\alpha(t) = \frac{1}{2t} \begin{pmatrix} \langle x^2(t) \rangle & \langle xy(t) \rangle & \langle xz(t) \rangle \\ \langle yx(t) \rangle & \langle y^2(t) \rangle & \langle yz(t) \rangle \\ \langle zx(t) \rangle & \langle zy(t) \rangle & \langle z^2(t) \rangle \end{pmatrix}, \quad (13)$$

where  $\alpha=w, wt, ot, o$ ; the brackets are defined in a particular manner—for instance,

$$\langle xy(t) \rangle = \frac{1}{N_p} \sum_{p=1}^{N_p} [x_n(t) - x_n(0)][y_n(t) - y_n(0)], \quad (14)$$

where  $x_n(t)$ ,  $y_n(t)$ , and  $z_n(t)$  are the coordinates of the diffusing particle  $n$  at time  $t$ . The total number of particles is  $N_p$ .

This tensor has known limits for long and short times. For long times, it is related to the macroscopic conductivity tensor  $\bar{\mathbf{D}}^\alpha$  in phase  $\alpha$  by

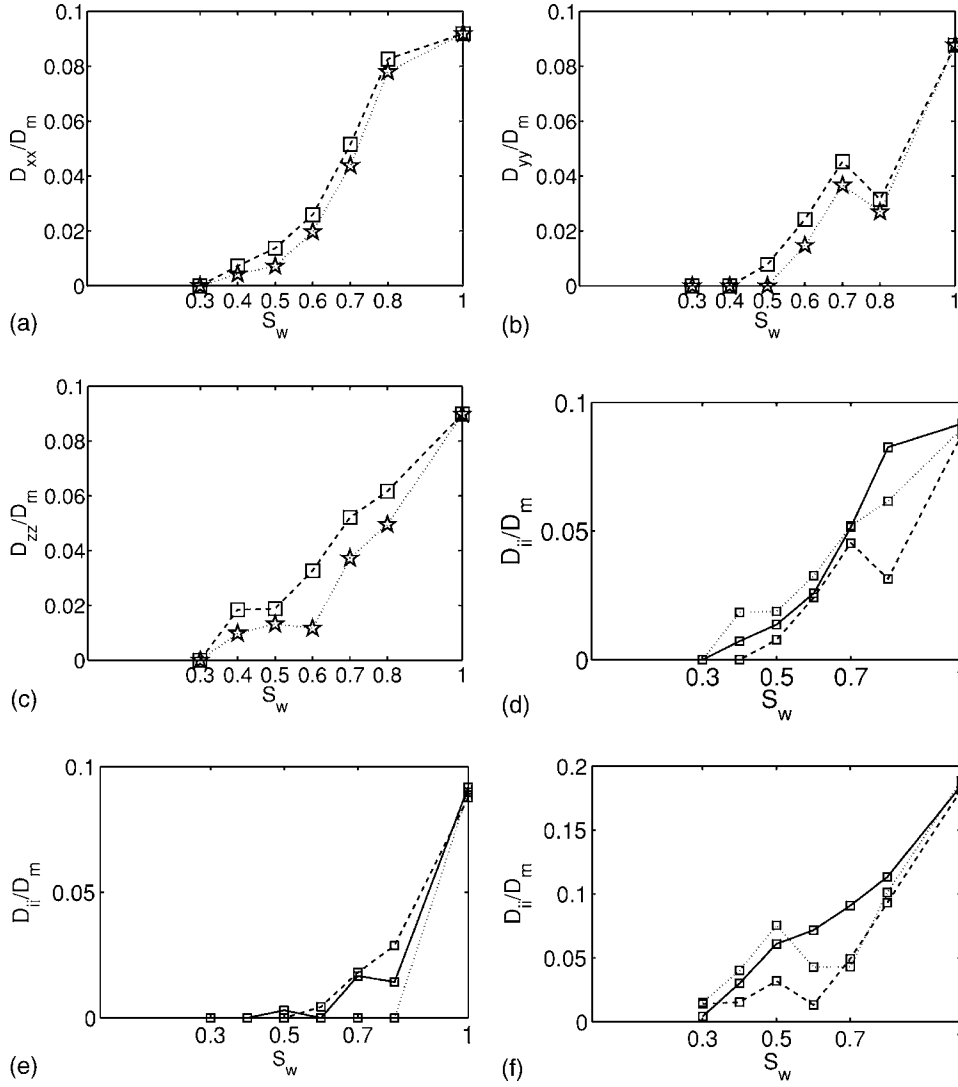


FIG. 4. The diagonal components of the conductivity tensor  $\bar{\mathbf{D}}/D_m$  for water for the sample  $\varepsilon=0.3$ . The components  $x$ ,  $y$ , and  $z$  are represented in (a), (b), and (c) for  $\alpha=w$  ( $\star$ , dotted line) and  $wt$  ( $\square$ , dashed line). The three components for  $\alpha=wt$  are superposed in (d):  $x$  (solid line),  $y$  (dashed line), and  $z$  (dotted line). For the samples  $\varepsilon=0.2$  and  $0.4$ , the three components for  $\alpha=wt$  are displayed in (e) and (f).

$$\lim_{t \rightarrow \infty} \mathbf{D}^\alpha(t) = \frac{\bar{\mathbf{D}}^\alpha}{\varepsilon S_\alpha}, \quad \alpha = w, o. \quad (15)$$

For short times and for isotropic porous media, [18] showed that

$$\frac{D(t)}{D_m} = 1 - \frac{4}{9\sqrt{\pi}} \frac{S}{V_p} \sqrt{D_m t} - \frac{S}{12V_p} \left\langle \frac{1}{R_1} + \frac{1}{R_2} \right\rangle D_m t + \frac{1}{6} \frac{\rho S}{V_p} D_m t + O((D_m t)^{3/2}). \quad (16)$$

This formula can be easily generalized to each phase  $\alpha$ .

### E. Numerical parameters of the simulations

The following parameters were used for the random walk simulations.

To be specific, the autodiffusion coefficient  $D_m$  of the fluid in the pore space was taken to be equal to  $2.58 \times 10^{-9}$  m<sup>2</sup>/s; the side  $a$  of the elementary cube used for the discretization of the media is equal to 5  $\mu$ m. Of course, these specific values are not essential; they just provide realistic orders of magnitude.

The time step  $\delta t$  is given by

$$\delta t = \frac{\delta_D^2}{6D_m}. \quad (17)$$

Generally speaking,  $N_p=10^6$  molecules were initially located in the samples.

Calculations were performed for the three porous media described in Sec. II A. Initial water saturation was varied between 0.3 and 0.8 by steps of 0.1.

Various dimensionless times are used for representing  $D(t)$ :

$$T_a^\alpha = \frac{\sqrt{D_m^\alpha t}}{a}, \quad (18a)$$

$$T_{I^\alpha} = \frac{4}{9\sqrt{\pi}} \frac{A^\alpha}{V^\alpha} \sqrt{D_m^\alpha t}, \quad (18b)$$

$$T_{\Lambda_i^\alpha} = \frac{D_m^\alpha t}{\Lambda_i^\alpha}, \quad (18c)$$

where  $\alpha=o, ot, wt, w$ . The subscript  $i$  indicates the direction—i.e.,  $i=x, y$ , or  $z$ .

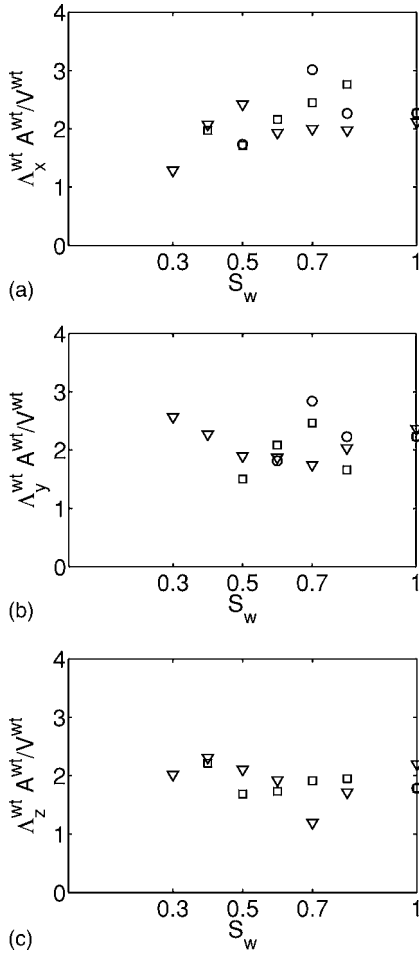


FIG. 5.  $\Lambda_i^{wt} A^{wt}/V^{wt}$  along the three space directions as a function of the saturation  $S_w$  for the three samples: (a) ( $i=x$ ), (b) ( $i=y$ ), and (c) ( $i=z$ ). Data are for  $\epsilon=0.2$  ( $\circ$ ),  $\epsilon=0.3$  ( $\square$ ), and  $\epsilon=0.4$  ( $\nabla$ ).

When expressed in terms of the dimensionless time  $T_{l\alpha}$ , Eq. (16) becomes

$$\frac{D_i^\alpha(T_{l\alpha})}{D_m^\alpha} = 1 - T_{l\alpha} + O((T_{l\alpha})^2), \quad i = x, y, z. \quad (19)$$

Since  $\Lambda_i'^\alpha = \sqrt{8K_{ii}^\alpha F_{ii}^\alpha}$  is a characteristic length of the porous medium analogous to  $l^\alpha = (A^\alpha/V^\alpha)^{-1}$ , the following representation is also useful:

$$D_i^w(T_{\Lambda_i'^\alpha}) = 1 - C_i T_{\Lambda_i'^\alpha} + O((T_{\Lambda_i'^\alpha})^2), \quad i = x, y, z. \quad (20)$$

### III. NUMERICAL RESULTS

#### A. Macroscopic properties

The permeability and conductivity tensors  $\mathbf{K}^\alpha$  and  $\overline{\mathbf{D}}^\alpha$  ( $\alpha=w, wt, ot, o$ ) were systematically calculated. Data for  $\overline{\mathbf{D}}^\alpha$  are summarized in Fig. 4.

Let us first note that generally speaking the nondiagonal terms are much smaller than the diagonal ones as expected for almost-isotropic-phase configurations. However, there are

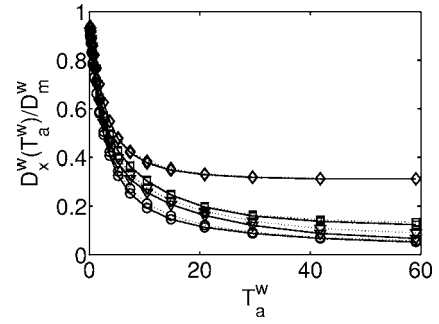


FIG. 6. The influence of the interfaces on the apparent diffusion coefficient  $D_{xx}(t)$  along the  $x$  direction for the sample  $\epsilon=0.3$ . The cases  $\alpha=w$  (solid line) and  $\alpha=wt$  (dotted line) are compared. Data are for  $S_w=0.4$  ( $\circ$ ),  $0.5$  ( $\nabla$ ),  $0.6$  ( $\square$ ), and  $0.8$  ( $\diamond$ ).

cases where this is not true; this occurs when the diagonal terms are significantly different—i.e., when the equilibrium configuration is anisotropic. Such an anisotropy may have two causes. First, the application of the pressure gradient breaks the isotropic character of the problem. Second, when the pressure gradient is set to zero, the configuration is changing under the action of the interfacial tension only and it has no reason to remain isotropic.

Results are detailed for the sample  $\epsilon=0.3$  for conductivity in Fig. 4. In (a), (b), and (c), the three diagonal components of the tensor are displayed for  $\alpha=w$  and  $wt$ . In most cases, except for  $D_{zz}^\alpha$ , the differences between the two “phases” are not significant though  $\overline{D_{ii}^w} < \overline{D_{ii}^{wt}}$  as expected on a physical basis. The three components for  $\alpha=wt$  are superposed in Fig.

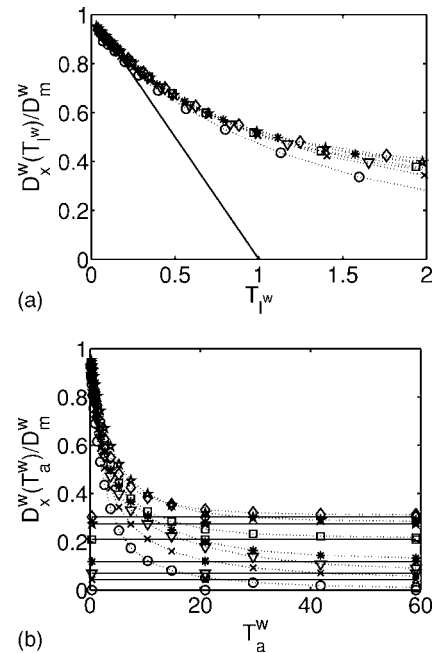


FIG. 7. Evolution of the apparent diffusion coefficient along the  $x$  direction for the sample  $\epsilon=0.3$  for short (a) and long (b) times. The water phase is defined by the majority rule. Data are for  $S_w=0.3$  ( $\circ$ ),  $0.4$  ( $\times$ ),  $0.5$  ( $\nabla$ ),  $0.6$  ( $*$ ),  $0.7$  ( $\square$ ),  $0.8$  ( $\diamond$ ), and  $1.0$  ( $\star$ ). The straight line in (a) is  $y(T_w)=1-T_w$ . The straight lines in (b) are obtained by the calculations defined in Sec. III A,  $\overline{D_{xx}^w}(\epsilon S_w D_m^w)$ .

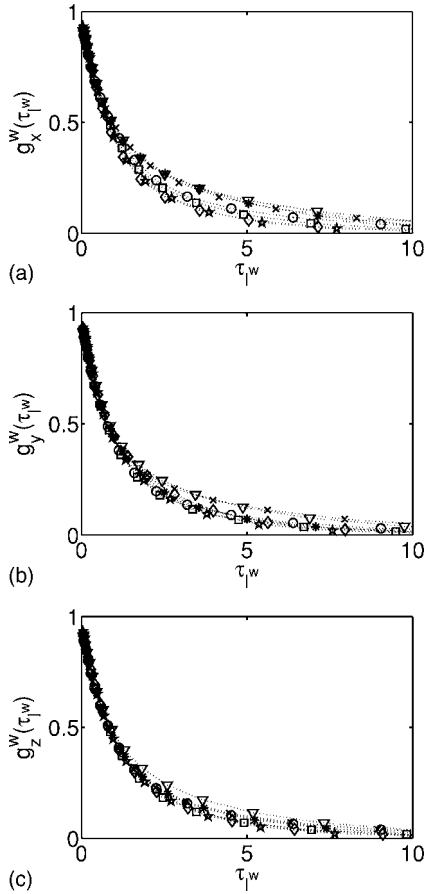


FIG. 8. The reduced representations  $g_i^w(\tau_{pw})$  ( $i=x,y,z$ ) of the apparent diffusion coefficient along the three spatial directions for the sample  $\varepsilon=0.3$ . The water phase is defined by the majority rule. Data are for  $S_w=0.3$  ( $\circ$ ),  $0.4$  ( $\times$ ),  $0.5$  ( $\nabla$ ),  $0.6$  ( $*$ ),  $0.7$  ( $\square$ ),  $0.8$  ( $\diamond$ ), and  $1.0$  ( $\star$ ). (a)  $g_x^w(\tau_{pw})$ , (b)  $g_y^w(\tau_{pw})$ , and (c)  $g_z^w(\tau_{pw})$ .

4(d); up to  $S_w=0.7$ , they are quite similar. This is not true anymore for  $S_w=0.8$ , while they are almost exactly the same for  $S_w=1$  since the porous medium itself was designed to be as isotropic as possible.

Results similar to Fig. 4(d) are displayed in Figs. 4(e) and 4(f) for  $\varepsilon=0.2$  and  $0.4$ . The three components do not superpose well for  $\varepsilon=0.2$ , and this feature is again verified for  $\varepsilon=0.4$ .

Equivalent data were obtained for permeability and comments are very similar to the ones given for conductivity.

Finally, the dimensionless parameter  $\Lambda^{wt}A^{wt}/V^{wt}$  was calculated for all the equilibrium configurations. Results are displayed in Fig. 5. As discussed by [6], it is expected that

$$\frac{\Lambda^{wt}A^{wt}}{V^{wt}} \sim 2 \quad (21)$$

if the electric field in the sample does not vary too much over the pore space. The data show that this relation is less well verified for two phases than for one phase. This quantity oscillates between 1 and 3 and can provide a first rough order of magnitude when needed. Otherwise there is no obvious trend with  $\varepsilon$  and  $S_w$ .

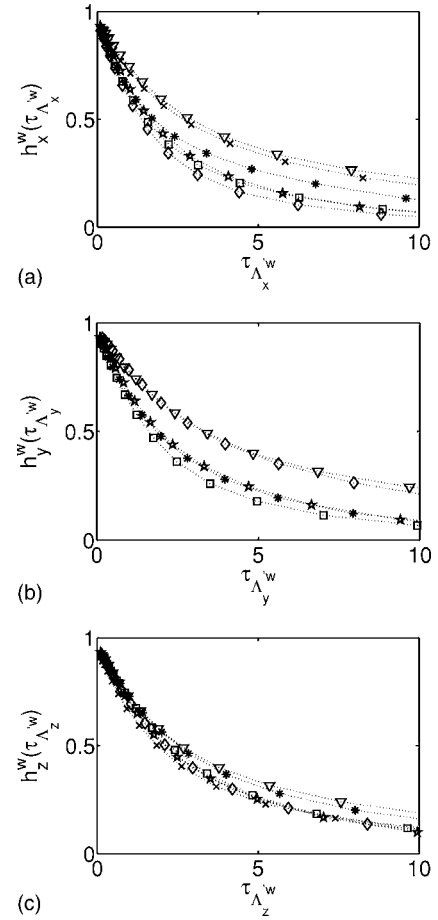


FIG. 9. The reduced representations  $h_i^w(\tau_{\Lambda_i^w})$  ( $i=x,y,z$ ) of the apparent diffusion coefficient along the three spatial directions for the sample  $\varepsilon=0.3$ . The water phase is defined by the majority rule. Data are for  $S_w=0.3$  ( $\circ$ ),  $0.4$  ( $\times$ ),  $0.5$  ( $\nabla$ ),  $0.6$  ( $*$ ),  $0.7$  ( $\square$ ),  $0.8$  ( $\diamond$ ), and  $1.0$  ( $\star$ ). (a)  $g_x^w(\tau_{\Lambda_x^w})$ , (b)  $g_y^w(\tau_{\Lambda_y^w})$ , and (c)  $g_z^w(\tau_{\Lambda_z^w})$ . The curves for which  $\Lambda_i^w=0$  are not plotted.

### B. Apparent diffusion coefficient in the water phase

The results obtained for the apparent diffusion coefficient are presented mostly for the sample with the intermediate porosity  $\varepsilon=0.3$ .

First, results obtained for  $\alpha=w$  and  $wt$  for a given direction are compared for various saturations in Fig. 6. As could be anticipated from Figs. 4(a)–4(c), the results are very similar. Because of this comparison, calculations are restricted to  $\alpha=wt$ ; i.e., the water phase is defined by the majority rule. Moreover, we shall follow the main lines of the presentation made by [6] for single phase flow.

Some results are presented for short times in Fig. 7(a). Because of Eq. (16), the data are expected to have a slope equal to  $-1$  at  $t=0$  when plotted in terms of  $T_{pw}$  [cf. Eqs. (18)]. Such a representation is seen to be very successful. The other known asymptote is for long times where the apparent diffusion coefficient should tend towards the limit expressed by Eq. (15). This behavior is illustrated in Fig. 7(b). It is again well verified. Similar results were obtained for the two other directions of space.

Finally, Valfouskaya *et al.* [6] showed that all the data relative to the apparent diffusion could be superposed on a

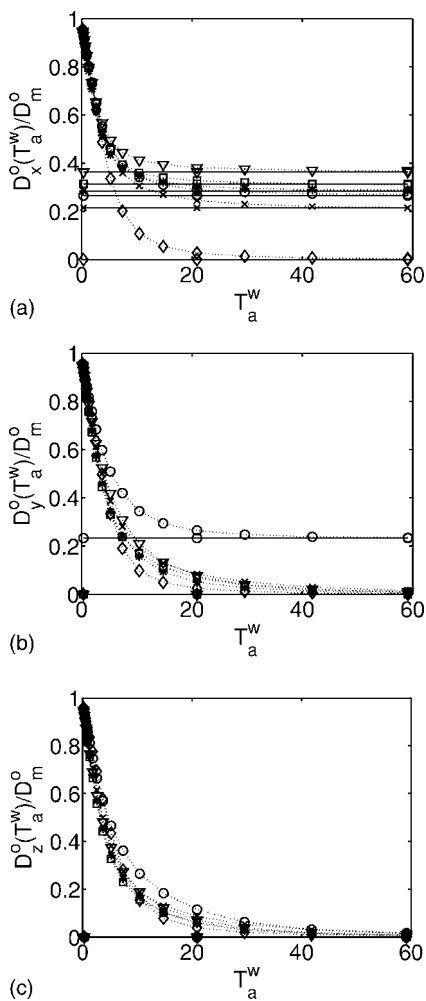


FIG. 10. The apparent diffusion coefficient along the three spatial directions for oil defined by the majority rule for the sample  $\varepsilon=0.3$ . Data are for  $S_w=0.3$  ( $\circ$ ),  $0.4$  ( $\times$ ),  $0.5$  ( $\nabla$ ),  $0.6$  ( $*$ ),  $0.7$  ( $\square$ ), and  $0.8$  ( $\diamond$ ). (a)  $D_x^o(T_a^w)/D_m^o$ , (b)  $D_y^o(T_a^w)/D_m^o$ , and (c)  $D_z^o(T_a^w)/D_m^o$ . The straight lines are obtained by the calculations defined in Sec. III A: (a)  $\bar{D}_{xx}^o/(\varepsilon S_o D_m^o)$ , (b)  $\bar{D}_{yy}^o/(\varepsilon S_o D_m^o)$ , and (c)  $\bar{D}_{zz}^o/(\varepsilon S_o D_m^o)$ .

single curve for very different porous media. In this purpose, recall the definitions

$$g_x^w(\tau_{pw}) = \frac{\frac{D_x^w(\tau_{pw})}{D_m^w} - \frac{1}{\alpha_x^w}}{1 - \frac{1}{\alpha_x^w}}, \quad (22a)$$

where

$$\tau_{pw} = \frac{T_{pw}}{1 - \frac{1}{\alpha_x^w}},$$

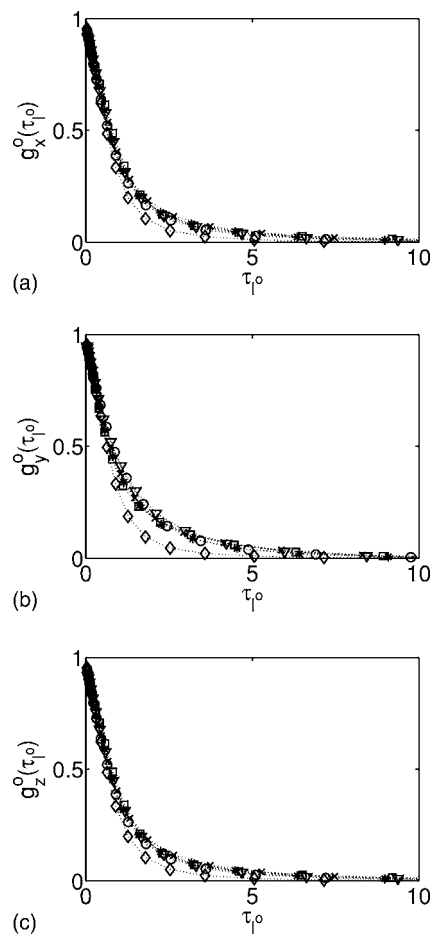


FIG. 11. The reduced representations  $g_i^o(\tau_{\rho})$ ,  $i=x,y,z$ , of the apparent diffusion coefficient along the three spatial directions for the sample  $\varepsilon=0.3$ . The oil phase is defined by the majority rule. Data are for  $S_w=0.3$  ( $\circ$ ),  $0.4$  ( $\times$ ),  $0.5$  ( $\nabla$ ),  $0.6$  ( $*$ ),  $0.7$  ( $\square$ ), and  $0.8$  ( $\diamond$ ). (a)  $g_x^o(\tau_{\rho})$ , (b)  $g_y^o(\tau_{\rho})$ , and (c)  $g_z^o(\tau_{\rho})$ .

$$h_x^w(\tau_{\Lambda_x^w}) = \frac{\frac{D_x^w(\tau_{\Lambda_x^w})}{D_m^w} - \frac{1}{\alpha_x^w}}{1 - \frac{1}{\alpha_x^w}}, \quad (22b)$$

where

$$\tau_{\Lambda_x^w} = \frac{T_{\Lambda_x^w}}{1 - \frac{1}{\alpha_x^w}},$$

where  $1/\alpha_x^w = \lim_{t \rightarrow \infty} D_x^w(t)/D_m^w = \bar{D}_{xx}^w/(\varepsilon S_o D_m^w)$  is the limit value of the apparent diffusion coefficient of phase  $\alpha$  along the  $x$  axis.

Let us consider the reduced curves  $g_i^w(\tau_{pw})$  and  $h_i^w(\tau_{\Lambda_i^w})$ ,  $i=x,y,z$ , displayed in Figs. 8 and 9. The curves  $g$  are reduced to a single one for  $g \geq 0.5$  for all three directions. Nevertheless, for smaller values of  $g$ , the curves separate. The curves for  $S_w=0.5$  are above the others for all directions. We observe also that the curves for  $S_w=0.4$  and  $0.6$  are also

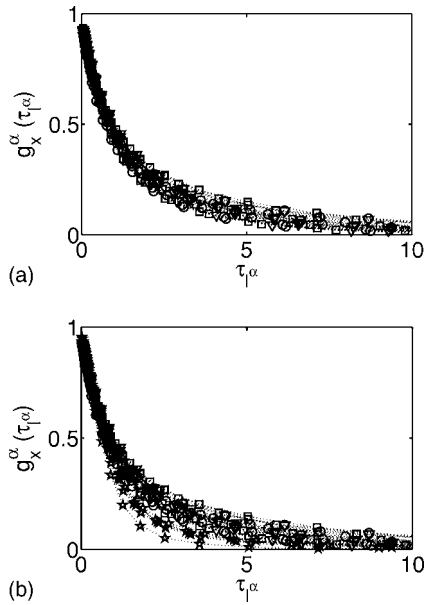


FIG. 12. The reduced representations  $g_x^\alpha(\tau_\alpha)$  of the apparent diffusion coefficient along the  $x$  direction for all the samples. (a) Diffusion in water for the three samples, (b) diffusion in water for the three samples and in oil for the sample  $\varepsilon=0.3$ . Data are for  $\alpha=wt$ ,  $\varepsilon=0.2$  ( $\circ$ ),  $\alpha=wt$ ,  $\varepsilon=0.3$  ( $\square$ ),  $\alpha=wt$ ,  $\varepsilon=0.4$  ( $\nabla$ ), and  $\alpha=ot$ ,  $\varepsilon=0.3$  ( $\star$ ).

above the others along the  $X$  direction [Fig. 8(a)]. Along the  $Y$  direction, it is the curve for  $S_w=0.4$ , and along the  $Z$  direction, it is the curve for  $S_w=0.6$  [Figs. 8(b) and 8(c)].

The reduced representations  $h$  are much worse than  $g$  along the  $X$  and  $Y$  directions [Figs. 9(a) and 9(b)]. The curves are separated almost from the very beginning. Along  $X$ , the curves for  $S_w=0.4$  and  $0.5$  are above the others. The curve for  $S_w=0.3$  cannot be taken into consideration since  $K_{xx}^w=0$  and, therefore,  $\Lambda_x'^w=0$ ;  $T_{\Lambda_x'^w}$  is not defined anymore. Along the  $Y$  direction, the curves for  $S_w=0.5$  and  $0.8$  are above the others, and for  $S_w=0.3, 0.4$ ,  $\Lambda_y'^w=0$ . As for  $Z$ , the curves are almost superposed for  $h \geq 0.5$  as for  $g$ . For  $h < 0.5$ , the curves are again separated. For  $S_w=0.5$  and  $0.6$ , they are above and for  $S_w=0.3$ ,  $\Lambda_z'^w=0$ .

The same calculations were performed for the other samples with very similar conclusions.

### C. Apparent diffusion coefficient in the oil phase

The apparent diffusion coefficient of oil is considered only for a sample of porosity  $\varepsilon=0.3$ . The limit values of the apparent diffusion coefficient for long times have no monotonic behavior with water saturation  $S_w$ .

The oil phase is often discontinuous, and this fact is captured by the apparent diffusion coefficient which tends to zero as illustrated in Fig. 10.

The reduced representations  $g_i^o(\tau_{i^o})$  are shown in Fig. 11. All the curves are well gathered for  $g_i^o > 0.5$  as for water. For larger values of the argument  $\tau_{i^o}$ , the curve  $S_w=0.8$  is below the others; for this saturation, oil does not percolate along any direction. Otherwise, the other curves fall onto a well defined curve.

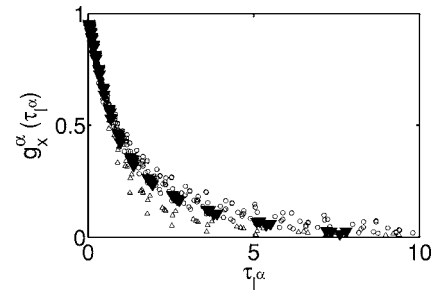


FIG. 13. Superposition of the reduced representations  $g_x^\alpha(\tau_\alpha)$ . ( $\circ$ ) water along the  $x$  direction for the samples  $\varepsilon=0.2, 0.3, 0.4$  for  $S_w \in [0.3, 1]$ . ( $\triangle$ ) oil for the sample  $\varepsilon=0.3$  for  $S_w \in [0.3, 0.8]$ . ( $\blacktriangledown$ ) average  $g_i^\alpha(\tau_{i^\alpha})$  ( $i=x, y, z$ ) along the three directions for single phase for the samples of porosities  $\varepsilon=0.2, 0.3, 0.4$ , and  $0.5$  (cf. Valfouskaya *et al.* [6]).

### D. Discussion

Let us now superpose the curves  $g$  obtained before for water in Fig. 12(a). It is seen that the superposition is excellent as a rule. It is even better than the superposition made in single phase for various classes of porous media [cf. Fig. (15a) of [6]]. Moreover, the curves  $g$  obtained for the three directions  $x$ ,  $y$ , and  $z$  for the sample  $\varepsilon=0.3$  can also be superposed.

Let us now superpose the data obtained for oil to the water data in Fig. 12(b). They are well superposed for short times, but the apparent diffusion coefficient is slightly smaller for oil for long times.

Finally, all the data obtained in single phase by [6], for water and oil in two phases are superposed in Fig. 13. The single-phase data are seen to fall in the middle of the two-phase data. Such an average position is expected on a physical basis.

Therefore, the apparent diffusion coefficients are quite close whatever the physical situation for values of  $g$  larger than  $0.5$  and (36a) of [6] still holds:

$$g_x^\alpha(\tau_\alpha = 0.75) = 0.5. \quad (23)$$

Such a relation can again be used to derive estimates of  $S^\alpha/V_p^\alpha$  and of  $K^\alpha$  in the conditions discussed in this reference.

### IV. CONCLUSION

NMR diffusion experiments without relaxation have been simulated in two phase equilibrium configurations calculated for reconstructed media. The porosity and water saturation parameters of these configurations were varied.

The actual fluid volumes and surface fluid-fluid and fluid-solid areas were calculated. Permeability and conductivity tensors as well as percolation property were determined. The influence of the interfaces where the two phases are mixed on these geometric and macroscopic properties has been studied.

The apparent diffusion coefficient was determined for each fluid. Its limit value for long times is not always monotonic with water saturation parameter. The apparent diffusion

coefficient tends to zero for a disconnected fluid phase with time.

The two major findings obtained for a single phase by [6] were confirmed for two phases. First, the ratio  $\Lambda^{wt}A^{wt}/V^{wt}$  was shown to be close to 2 whatever the porosity and saturation. Second, the reduced curve  $g(\tau_l)$  gathers the data obtained for both phases. This curve is very close to the one

obtained by [6] for a single phase and for the same reconstructed unimodal porous media.

Thanks to the versatility of the random walks numerical code, the present study can be easily extended to other real physical situations. For instance, relaxation can be simulated at the interfaces between each fluid and solid and between the fluid molecules of the bulk fluid, to name a few.

- 
- [1] D. L. Johnson, J. Koplik, and L. Schwartz, *Phys. Rev. Lett.* **57**, 2564 (1986).
- [2] J. J. Tessier and K. J. Packer, *Phys. Fluids* **10**, 75 (1998).
- [3] R. L. Kleinberg, in *Methods in the Physics of Porous Media*, edited by P. Wong (Academic, San Diego, 1999).
- [4] S. Godefroy, Ph.D. thesis, École Polytechnique, Paris, 2001.
- [5] E. Toumelin, C. Torres-Verdin, and S. Chen, *SPE Reservoir Eval. Eng.* **6**, 234 (2003).
- [6] A. M. Valfouskaya, P. M. Adler, J.-F. Thovert, and M. Fleury, *J. Appl. Phys.* **97**, 1 (2005).
- [7] A. K. Gustensen, Ph.D. thesis, Massachusetts Institute of Technology, 1992.
- [8] I. Ginzbourg and P. M. Adler, *J. Phys. I* **4**, 191 (1995).
- [9] P. M. Adler, C. G. Jacquin, and J. A. Quiblier, *J. Phys. (Paris)* **16**, 691 (1990).
- [10] J.-F. Thovert, F. Yousefian, P. Spanne, C. G. Jacquin, and P. M. Adler, *Phys. Rev. E* **63**, 061307 (2001).
- [11] V. V. Mourzenko, J.-F. Thovert, and P. M. Adler, *Eur. Phys. J. B* **19**, 75 (2001).
- [12] A. Moctezuma-Berthier, O. Vizika, J.-F. Thovert, and P. M. Adler, *Transp. Porous Media* **56**, 225 (2004).
- [13] S. Békri, J. Howard, J. Muller, and P. M. Adler, *Transp. Porous Media* **51**, 41 (2003).
- [14] R. Lemaître and P. M. Adler, *Transp. Porous Media* **56**, 325 (1990).
- [15] J.-F. Thovert, F. Wary, and P. M. Adler, *J. Appl. Phys.* **68**, 3872 (1990).
- [16] N. Martys and E. J. Garboczi, *Phys. Rev. B* **46**, 6080 (1992).
- [17] D. B. Pengra, S. Li, S. X. Li, and P. Z. Wong, in *Dynamics in Small Confining Systems*, edited by J. M. Drake, J. Klafter, K. Kopelman, and S. M. Troian, *Mater. Res. Soc. Symp. Proc. No. 366* (Materials Research Society, Pittsburgh, 1995).
- [18] P. P. Mitra, P. N. Sen, and L. M. Schwartz, *Phys. Rev. B* **47**, 8565 (1993).